

Chapter 6

Applications de la Combinaison des Techniques de *Fast-Marching* et de *Level-Sets* à l'Extraction de Surface

Résumé — Dans ce chapitre, nous avons étudié deux problèmes où la mesure et la visualisation du résultat de la segmentation sont primordiales.

Tout d'abord, on a étudié les anévrismes du cerveau, qui sont des gonflements des artères, qui peuvent mener à une hémorragie cérébrale et plonger le patient dans le coma. Dans ce cas, c'est la précision et la rapidité de la segmentation qui sont des éléments fondamentaux pour préparer une intervention chirurgicale.

Le second problème est celui des polypes du colon. Dans le cas de la colonoscopie virtuelle de la section 3.1, l'utilisateur regarde l'intérieur du colon, et la détection des polypes repose entièrement sur ses indications. Nous avons utilisé notre méthode de segmentation pour automatiser et rendre robuste cette tâche de détection en améliorant la visualisation.

Abstract — In this chapter, we have studied two different problems related to typical pathologies, where measurements and visualization are the main objectives. First problem is the segmentation of cerebral aneurysm which are dilation of the brain vessels that may burst and lead to coma. Accuracy and speed of the segmentation process are needed in order to prepare interventional treatment. We therefore applied successfully our methods to segment and extract a shape representation of cerebral aneurysms.

Second problem is the already studied colon polyps visualization. In virtual colonoscopy, as developed in section 3.1, the user observe the interior of the colon, and detection is based on its indications. We want to automate this task, and we give preliminary results on an interesting visualization mode that could lead to this target.

6.1 Segmentation of cerebral aneurysms

What is an aneurysm?

An aneurysm is an abnormal dilatation involving the wall of an artery, a thick-walled blood vessels that carry blood pumped from the heart, under high pressure. Aneurysms can develop on any artery within the body. Common arteries where aneurysms are found include the aorta, the popliteal artery (behind the knee) and brain arteries. We focus on the brain aneurysms (see figure 6.3-right). A brain aneurysm begins as a small thinned area at the wall of an artery at the base of the brain (see figure 6.1). Over time the blood flow pounds against the thinned portion

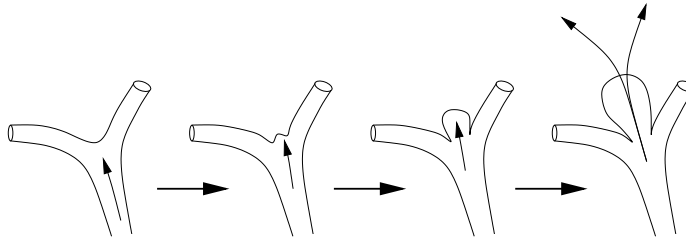


Figure 6.1. Development and rupture of a brain aneurysm: The blood flow, represented by an arrow, stresses an area of “potential” weakness at the branching point of an artery. Over time, this point of weakness dilates into an aneurysm. The blood enters the aneurysm itself and finally escapes from a rupture point at the top of the aneurysm.

of the wall, and eventually it starts to dilate, inflating like a balloon, creating the aneurysm, and as it grows, the wall of the artery gets thinner and thinner, until it ruptures.

What causes an aneurysm to form?

This is still an open question. Aneurysms arise at an area where the wall of an artery is thin. Most arteries in the body have walls with three layers, and brain arteries have segments where one of the layer is absent, which can contribute to the problem. An aneurysm may be caused or aggravated by disease such as hypertension, because it results in high blood pressure, or may be caused by any disease which affects the walls of the arteries (even smoking).

What dangers do aneurysms present?

The danger from an aneurysm is that it will continue to bulge and may burst. When an aneurysm in a large blood vessel or in the heart bursts, a person could bleed to death. When an aneurysm bursts in the brain, a stroke (brain attack) can result.

How are cerebral aneurysms diagnosed?

Biplane angiography has become a standard imaging procedure for the treatment of cerebral aneurysms. Recently, there has been a lot of interest in 3D visualization of intracranial vessels in interventional neuroradiology [95]. A clinical application of 3D-Rotational Angiography (**3D-RA**) has been developed by Philips, using a standard angiographic system, with a C-arm that performs a rotational angiographic

acquisition around the patient, and provide accurate 3D reconstruction [45]. With classical rendering techniques, it enables the clinician to observe for example the relationship of a parent vessel with the neck of an aneurysm, in the brain vessels. The availability of three-dimensional information during the intervention increase the possibilities towards a more accurate and time efficient endovascular treatment. With volume rendering tools, the clinician is able to see structures from any angle. But still, it relies on threshold-based visualizations techniques.

How are cerebral aneurysms treated?

There are two ways to treat an aneurysm: First one is surgical treatment, where the clinician places the patient under general anesthesia. A window is opened in the skull bone of the patient head. When the aneurysm is in view, it is separated from the surroundings structures by dissection, and a metal clip is closed across the base of the aneurysm. Therefore blood no longer flow into the aneurysm (see figure 6.2-middle). Second way is to do endovascular coiling: this technique consists of filling the

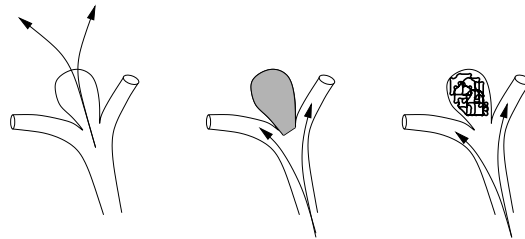


Figure 6.2. Treatment of a brain aneurysm: Left image shows an aneurysm at a branch point; middle image illustrates the placement of a clip across the base of an aneurysm correctly placed; right image illustrates the packing of the same aneurysms with coils.

aneurysm from the inside with a long length of fine platinum wire that coils around and around inside the aneurysm, until the blood flow stops entering the aneurysm (see figure 6.2-right). In order to reach the aneurysm, the clinician puts a fine catheter through the artery, and advances it into the head until it reaches the aneurysm. Then the wire is passed up into the catheter and into the aneurysm, until it is full of wire. This treatment has its own risks and complications, since it is still a very invasive technique. The aneurysm can burst during the treatment. In order to perform this examination in the best condition, the clinician needs to output from the angiography an accurate model of the aneurysm. The surface of the object segmented can be used to do measurements, but also flow simulations in order to determine critical points of possible rupture.

We have applied the segmentation models used in section 5.4, in order to increase the accuracy of the visualization of the pathologies. Increasing accuracy and speed of the computations is important for a system in an interventional environment. The 3D shape information will enhance analysis of the structures, measure of the vascular anatomy, and preparation of the treatment.

6.1.1 Description of the acquisition system

The system uses a standard angiographic system that is equipped with an image intensifier on a C-arm which performs a rotational angiographic acquisition over a range of 180° (see figure 6.3-middle), scanning 100 projection images. The clinician injects



Figure 6.3. 3D Rotational Angiography (3D-RA) System: Rotating around the patient, as shown in right image, the system acquire 100 projections along the half circular trajectory, as shown on the middle image; right image is a threshold-based volume rendering of a cerebral aneurysm computed from the 3D dataset reconstructed.

contrast product in the vessel during the acquisition (300 mg/ml iodinated contrast agent at a flow rate of 4-5 ml/s), to fill the pathology of interest during the scan. Acquired scans are then transferred to a workstation, and are automatically corrected for the image intensifier distortion, according to an initial performed calibration step. The reconstruction of the rotational images into a volume is performed by a modified version of the cone-beam algorithm of *Feldkamp* [51] (because of the half-circular trajectory). The default reconstruction procedure, from acquisition until the 3D volume creation takes approximately 6 minutes. And the 3D result can be viewed with a real-time volume rendering package (see figure 6.3-right).

6.1.2 Application to the segmentation of brain aneurysms

Threshold-based volume rendering is not sufficient to correctly extract valuable information from the dataset acquired (see figure 6.4 a cerebral aneurysm data, and its **MIP** projection image).

On complex objects, the topology will vary according to the selected visualization threshold on the raw volume. Some vessels will merge, and others split. It appears unreliable to visualize raw reconstructed volumes in terms of topology and vessel size.

We apply the competitive front method, described in section 5.3 to this kind of dataset, in order to operate a supervised fast pre-segmentation of the dataset. Only requirement is to set a seed region inside the object of interest, and another one in the background. The contrast-filled object being clearly bright on the dataset, it is not difficult at all to select a voxel v_{in} inside the aneurysm, and another voxel v_{out} outside it. Using our formulation of two propagating fronts \mathcal{F}_{in} and \mathcal{F}_{out} with two different initial penalty functions $\mathcal{P}_{in}^0 = \mathcal{I}(v_{in})$ and $\mathcal{P}_{out}^0 = \mathcal{I}(v_{out})$ lead to the segmentation shown in first row of figure 6.6. When the two fronts collides at time t ,

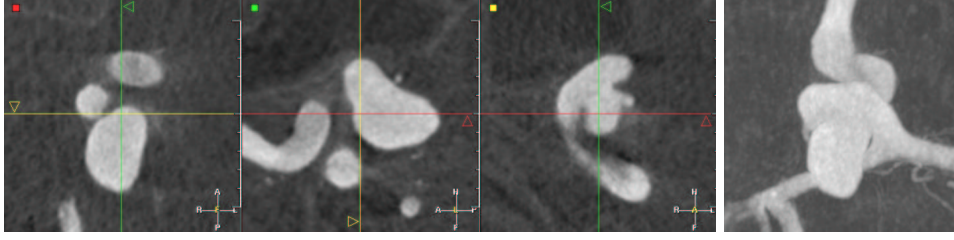


Figure 6.4. Example of 3D-RA dataset: The left image represents three orthogonal views of a cerebral aneurysm acquired with the **3D-RA** system; right image is a MIP of this dataset.

the new penalty \mathcal{P}_{in}^t and \mathcal{P}_{out}^t are input in our region-based geodesic active contour framework. Knowing the two distributions (μ_{in}, σ_{in}) and $(\mu_{out}, \sigma_{out})$, and that the aneurysms are brighter than the background, we initialize the region descriptors with the region following region probabilities:

$$\mathcal{P}_{in}(x, t) = \begin{cases} \frac{1}{\sqrt{2\pi}\sigma_{in}(t)} \exp\left(-\frac{(\mathcal{I}(x) - \mu_{in}(t))^2}{2\sigma_{in}^2(t)}\right) & \text{if } \mathcal{I}(x) < \mu_{in}(t) \\ \frac{1}{\sqrt{2\pi}\sigma_{in}(t)} & \text{if } \mathcal{I}(x) \geq \mu_{in}(t) \end{cases}$$

$$\mathcal{P}_{out}(x, t) = \begin{cases} \frac{1}{\sqrt{2\pi}\sigma_{out}(t)} & \text{if } \mathcal{I}(x) < \mu_{out}(t) \\ \frac{1}{\sqrt{2\pi}\sigma_{out}(t)} \exp\left(-\frac{(\mathcal{I}(x) - \mu_{out}(t))^2}{2\sigma_{out}^2(t)}\right) & \text{if } \mathcal{I}(x) \geq \mu_{out}(t) \end{cases}$$

The corresponding descriptors are shown in figure 6.5-right.

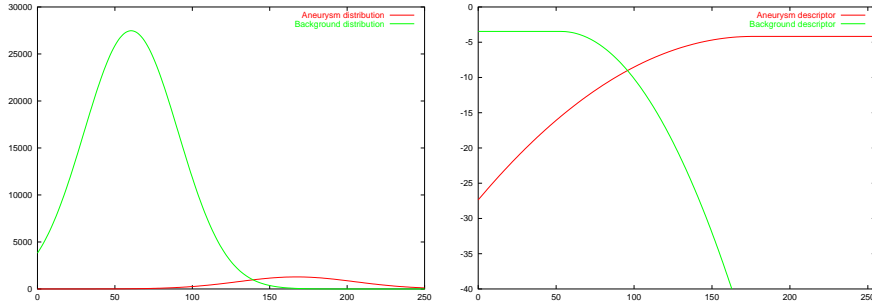


Figure 6.5. Region descriptors for the 3D-RA image: Left image shows the estimated Gaussian distribution of the inside and the outside of the cerebral aneurysm segmented by *Fast-Marching* as shown in first row in figure 6.4; the inside $\rightsquigarrow \mathcal{N}(167, 37)$ and the background $\rightsquigarrow \mathcal{N}(60, 30)$.

Using the region descriptors k_{in} and k_{out} in the model defined in section 5.2, we iterate 20 times from the *Fast-Marching* initialization, to the final segmentation, shown in second row of figure 6.6.

The variability in positioning the initial seed voxels inside and outside the object does not have a clear impact on the final solution, since it provides an initial guess,

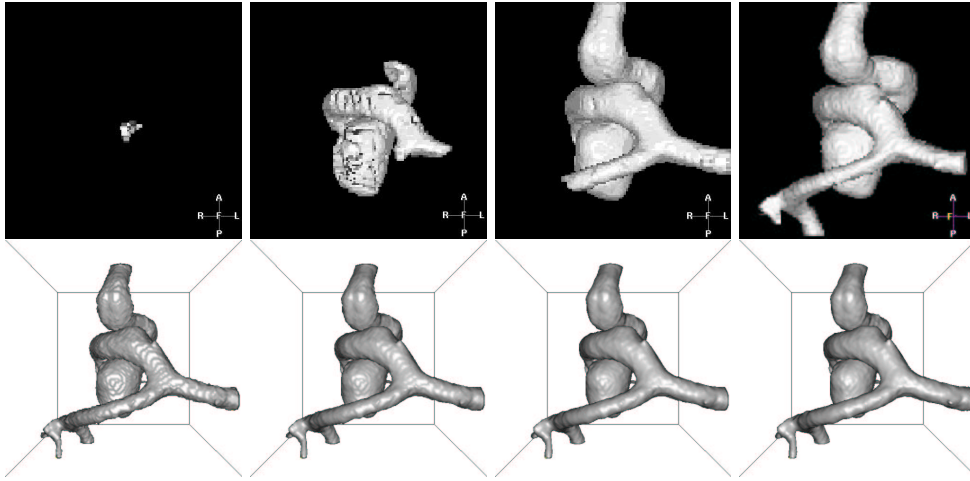


Figure 6.6. Example of brain vessels segmentation with combination of Fast-Marching and Level-Sets: First row shows iterations of the segmentation process described in section 5.3; second row shows iterations of the final refinement technique described in section 5.4; parameters for inside object $\alpha = \eta = .8$ and $\zeta = 0.05$.

near the final converged zero level-set, and since it is the initialization of the region-based descriptors. The independence of the region-based level-set framework from the initialization ensures that variability in setting the initial seeds.

The measure of the variability of the positioning of the seed point, whereas it does not have any clear impact on the final result, should be emphasized, since it is the initialization of the region-based descriptors. The variation in the acquisition protocol could optimized the settings of parameters of the boundary based forces, towards region-based forces importance.

And the setting of the seed points could be automated, since the dataset is centered in the volume of interest, and it always intersects the image borders (the intersection could be recognized, being the section of a circular vessel).

The same process, including supervised pre-segmentation and automatic final segmentation was applied to a set of cerebral aneurysms see figure 6.7. The descriptors k_{in} and k_{out} issued from the segmentation model of the cerebral aneurysm of figure 6.4 were used for each dataset. The boundary descriptors attracted the zero-level set of ϕ and converges rapidly. Parameterization was the same for each dataset, and stability of the protocol ensured fast convergence to the aneurysms shown in last row of figure 6.6.

The shape extraction of the aneurysm is done in less than 2 minutes on a 300MHz Sun Workstation. Knowing that the reconstruction procedure, from acquisition until the 3D volume creation takes 6 minutes, the added procedure value towards its cost is not important, especially if we consider that on a classical standard commercial PC, this cost could be divided by two. Therefore, this procedure provides all the

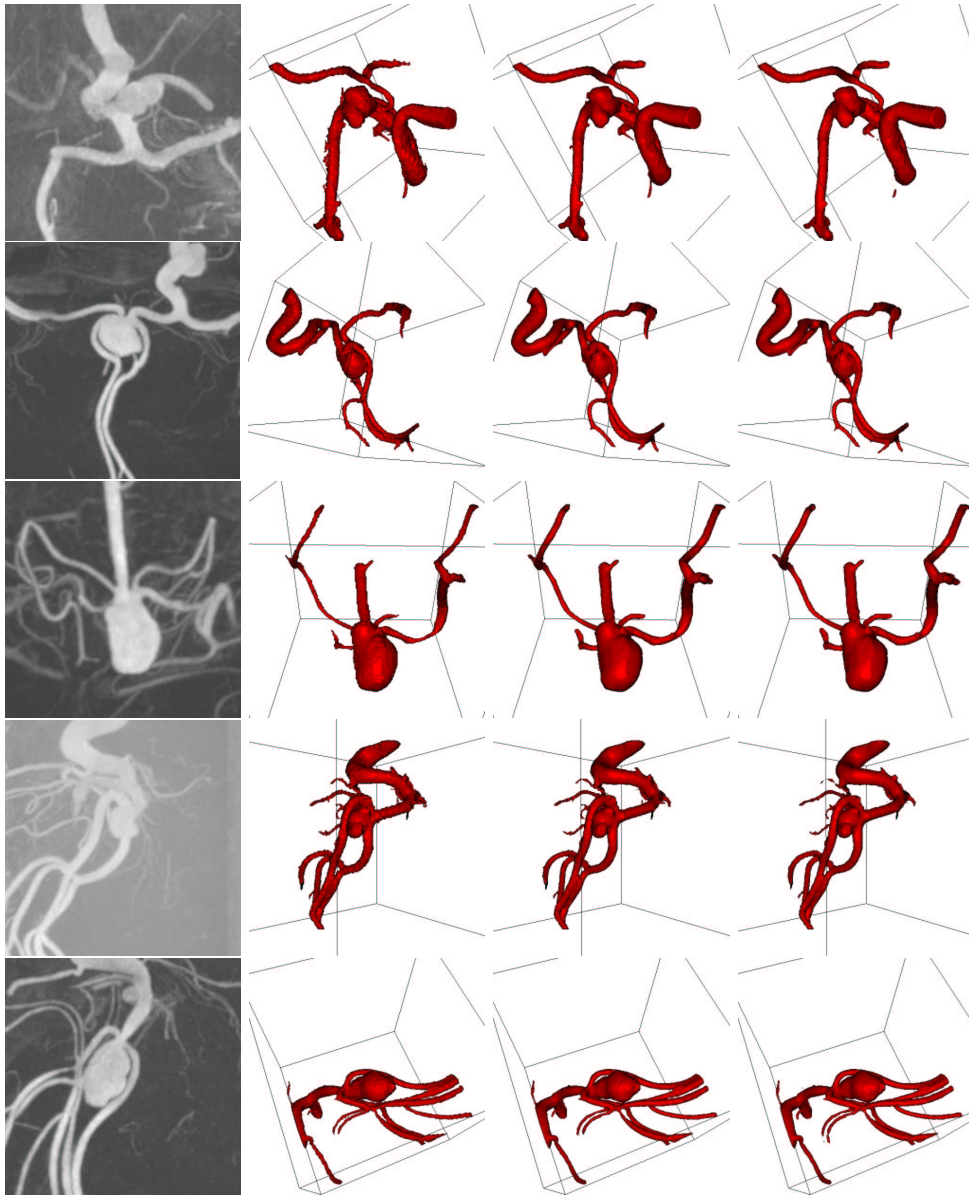


Figure 6.7. Segmentation of five 3D-RA datasets: First column contains the MIP images of the five data-sets; The surface rendered views show, from left to right in each row, iterations 0, 10 and 20 of the level-set segmentation process.

anatomical information required for the entire course of endovascular treatment of cerebral aneurysms. Direct benefits for interventional neuroradiology:

1. fast and accurate analysis of the morphology of the aneurysms, including determination of the size and the relationship with the parent vessel, allowing selection of the appropriate stent size, catheter and guide-wire thickness, or coil length;
2. fast and safe decision regarding the feasibility of endovascular approach.
3. to reduce radiation exposure: **DSA** images are still the gold standard in Angiography during interventional treatment, but when the 3D result is available, less 2D images need to be acquired before, during, and after the treatment;

6.1.3 Perspective

The 3D shape representation of the aneurysms creates lots of investigation fields. In particular we could reduce (or suppress) contrast agent injection: the 3D model could be mapped/projected on the 2D image during intervention, by registration techniques, and used as a mask for the treatment (see figure 6.8);

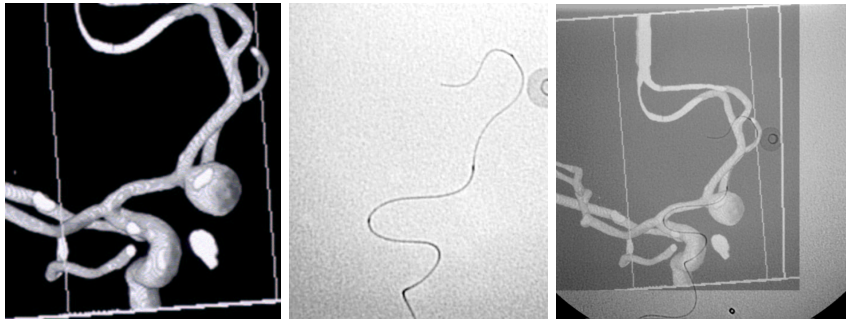


Figure 6.8. Live road mapping for interventional treatment: Left image is a 3D threshold based volume rendering; middle image is a 2D X-ray image of a guide and a catheter; right image is the superposition of those 2 images.

Another research direction could be the road-mapping of interventional treatment: the segmentation of the vessel structure enables to extract trajectories inside the vasculature, in order to efficiently reach the aneurysm (for stent placement for example), forecasting the future problems during intervention. Path extraction techniques, studied in chapter 2, could also be useful for extracting the optimal guide shape for an intervention: during intervention, for glue injection, the clinician introduces the catheter in the aneurysm, with the help of the guide. Then when the guide is extracted, the catheter - similar to a spaghetti - can move out the aneurysm, or eventually break it. This dangerous step can be avoided if the catheter has been optimally shaped using a trajectory artificially extracted in the 3D model.

Finally, the explicit surface extracted from the *Level-Sets* representation (with the *Marching-Cubes* algorithm) is a mesh that enables modeling of the blood flow inside the aneurysm. This model can help in preventing bursting of the aneurysms, but could be also very useful in following-up the result of an intervention.

6.2 Detection of Colon Polyps

This problem was already mentioned in section 3.1, concerning the path extraction tool developed specifically for virtual endoscopy. As said, colorectal cancer represents the third most frequently diagnosed cancer worldwide. If we consider malignant tumor, the yearly incidence of colorectal cancer probably approaches 160,000 cases [99]. This disease begins in the cells that line the colon, as polyps.

What is a Colon Polyp?

A polyp is a growth that occurs in the colon and other organs. These growths, or fleshy tumors, are shaped like a mushroom or a dome-like button, and occur on the inside lining of the colon.

What dangers do polyps present?

Colon polyps start out as benign tumors but in time may become malignant. The larger the polyp, the more likely it is to contain cancer cells.

Why do Colon Polyps and Cancer Form?

A great deal is known about why and how polyps form. There now is strong medical evidence that there are abnormal genes for colon polyps and cancer that can be passed from parent to child. Diet and foods may also be very important.

How are Colon Polyps diagnosed?

Importantly, colon cancer is one of the most curable forms of cancer. When detected early, more than 90 percent of patients can be cured. Early detection of colon polyps and cancer is performed usually with

1. study of the patient's medical history for identification of risk factors;
2. stool examination to detect occult blood from Colon cancers and large polyps;
3. visual examination of the lower colon using a lighted, flexible endoscope;
4. colonoscopy of the entire 5-6 foot long colon, under sedation;
5. x-ray exam (Barium Enema) which outlines the shadows of polyps and cancer;
6. virtual colonoscopy (already developed in section 3.1).

But still, even the *Virtual Endoscopy* relies on the user observation, for the detection, during visualization, of possible polyp existence. We already mentioned a possible unfolded view of the interior of the colon (see figure 3.21) that enables to see in all directions while traveling through the colon, but inspection remains a supervised process that rely on possible miss of hidden regions, from the camera point of view. Last drawback of endoscopy is that it relies on the choice of an opacity threshold input in the volume-rendering tool. The choice of this threshold critically constrain the position of the colon surface, thus the clinical validity of the observation.

6.2.1 Segmentation of the colon surface

We propose in the following to adapt the method developed in previous chapter, and already applied to cerebral aneurysm segmentation, to develop a initial framework of

semi-automatic polyp extraction. We further explore possibilities of detection with visualization techniques, using the curvature information of the object surface.

Classical CT scanner are generally very large. Instead of treating entire images, we used small volumes of interest which were selected by specialized physicians because of the presence of a particular pathology.

Before acquisition, the patient goes through a particular preparation during which the colon is emptied as much as possible. During the scan it is distended by inflating room air. The resulting image intensity in the colon lumen is rather uniform and lower than in the rest of the image, with a relatively good contrast. Therefore, the critical step of the segmentation process is the variability of the topology and geometry of the pathological structures.

Since the contrast is really important, as shown in figure 6.9-(a), it is a very easy task to set a seed point inside the colon, and another outside. Thus, supervised seg-

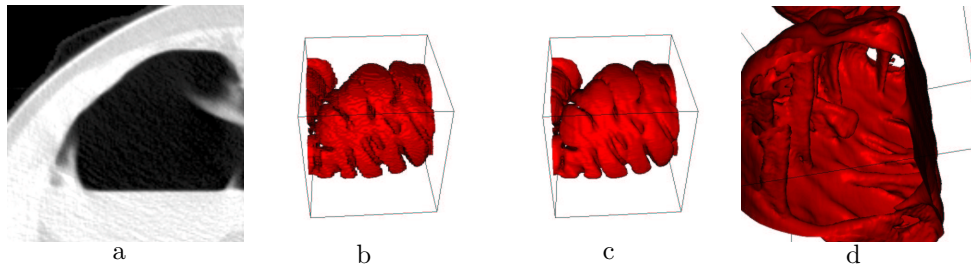


Figure 6.9. Example of polyps Segmentation: image (a) is a slice of a volume of interest (VOI) of the 3D CT scanner of the colon studied; image (b) shows the resulting pre-segmentation obtained with the *Fast-Marching* competitive version; image (c) is the result of the region-based *Level-Sets* at convergence, after 20 iterations; image (d) is an endoluminal view of the same segmented object, which emphasizes the polyps that grows on a fold of the colon surface.

mentation with front competition, using the *Fast-Marching* as detailed in section 5.3, can be easily achieved, as shown in figure 6.9-(b). Using the descriptors output by the pre-segmentation process, we initialize our *Level-Sets* with sigmoidal region-based forces. The justification of the use of those forces is the following: Pathological cases can arise, as shown in figure 6.10 In this application, the use of sigmoidal region-based forces is interesting because, due to the topology of the colon, that intersects several times the same volume of interest, it is possible to obtain disconnected parts of the colon in the same volume. Pre-segmentation being based on the setting of an interior seed point and an exterior seed point will lead to a binary image. This means that portions of the colon are probably included in the background. Therefore the statistical study of the background grey-levels will lead, with the Gaussian descriptors, to a background that have a large variance (see figure 6.11-left), whereas local histogram in the colon, due to the contrast, will give a small variance. Values for the example shown in figure 6.10-a, are $(\mu_{in} = 40, \sigma_{in} = 23)$ for the colon, and $(\mu_{out} = 620, \sigma_{out} = 385)$ for the background. Unless the user finds all disconnected parts of the colon, it is easier to use the *choice* of a darker region for the colon, and a brighter one, for the background, since evolution of the Gaussian model could lead to

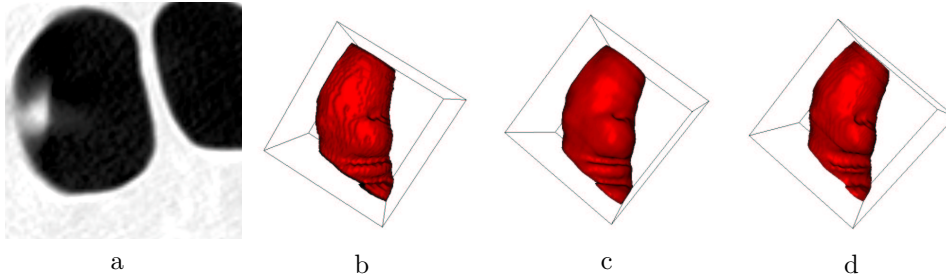


Figure 6.10. Segmentation tests with different descriptors: image a is the underlying dataset; image b is the initialization with the *Fast-Marching* algorithm; image c is the resulting segmentation after 100 iterations of the *Level-Sets* sigmoid region based forces; image d is the similar segmentation with Gaussian region based forces.

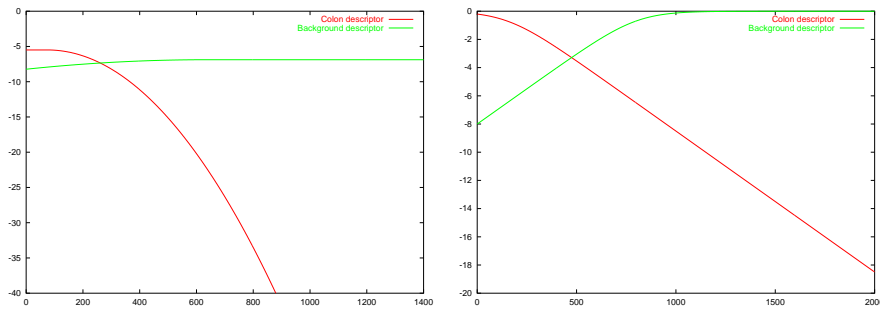


Figure 6.11. Region descriptors for the colon polyps: The left image represents the thresholded Gaussian descriptors for the colon polyps of figure 6.9; right image corresponds to the sigmoid descriptors of the same dataset.

unexpected results. In figure 6.10-4, the colon surface is flattened across iterations, because the variance of the background is higher. In figure 6.12, we display the result of the application of the same framework, using the same parameters than for example 6.9.

6.2.2 Visualization of the colon polyps

Colon polyps appear as convex regions in the lumen surface, in intraluminal 3D views (see segmentation results in figure 6.12). We tried to enhanced these suspect regions using a color information on the surface.

The specific shape of the colon polyps settle the use of the curvature information, mapped on the surface of the object, using an adequate color-map to highlight the cups. This technique has been already used in the surface of a segmented cortex, by *Zengh et al.* [195], using a measure defined originally by *Koenderink et al.* [94]. Using the values of ϕ , $\phi(\cdot, t)$ at convergence, we know the expressions of the mean curvature κ_M and the Gaussian curvature κ_G for a surface propagating in three space

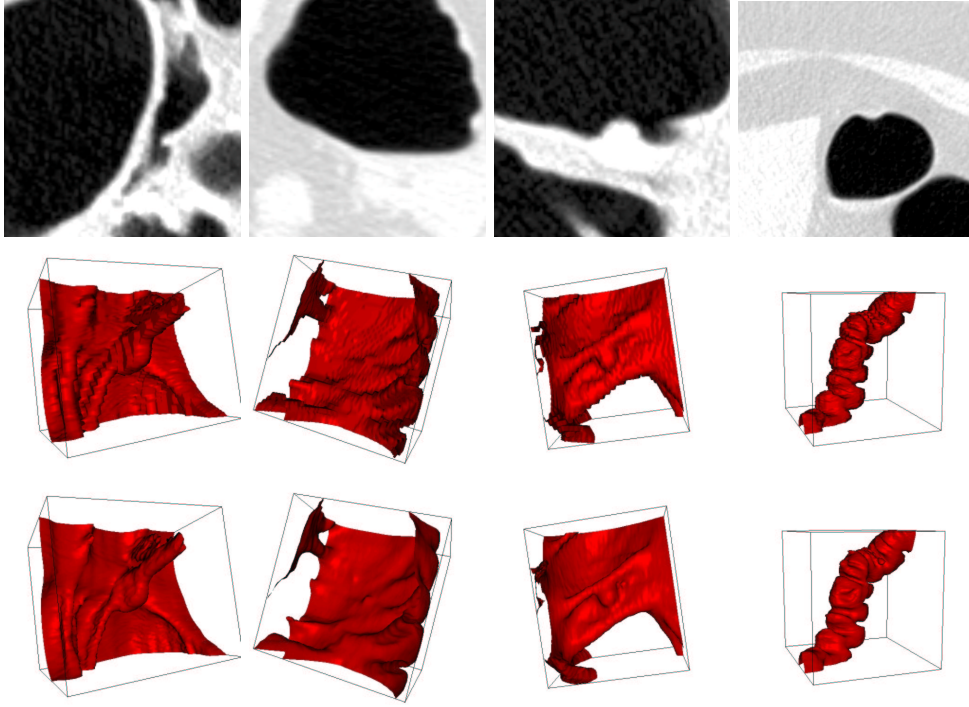


Figure 6.12. Polyps segmentation: First row: the four datasets used for segmentation; second row: the respective initializations given by the Fast-Marching competition algorithm described in section 5.3; third row: visualization after 20 iterations with region-based forces of the respective zero level-set.

dimension, in terms of the level-set function $\tilde{\phi}$. They can be easily computed using formulations given by *Sethian* [163]:

$$\kappa_M = \nabla \cdot \frac{\nabla \tilde{\phi}}{|\nabla \tilde{\phi}|} = \frac{\begin{Bmatrix} (\tilde{\phi}_{yy} + \tilde{\phi}_{zz})\tilde{\phi}_x^2 + (\tilde{\phi}_{xx} + \tilde{\phi}_{zz})\tilde{\phi}_y^2 + (\tilde{\phi}_{yy} + \tilde{\phi}_{xx})\tilde{\phi}_z^2 \\ -2\tilde{\phi}_x\tilde{\phi}_y\tilde{\phi}_{xy} - 2\tilde{\phi}_x\tilde{\phi}_z\tilde{\phi}_{xz} - 2\tilde{\phi}_y\tilde{\phi}_z\tilde{\phi}_{yz} \end{Bmatrix}}{(\tilde{\phi}_x^2 + \tilde{\phi}_y^2 + \tilde{\phi}_z^2)^{3/2}} \quad (6.1)$$

$$\kappa_G = \frac{\begin{Bmatrix} \tilde{\phi}_x^2(\tilde{\phi}_{yy}\tilde{\phi}_{zz} - \tilde{\phi}_{yz}^2) + \tilde{\phi}_y^2(\tilde{\phi}_{xx}\tilde{\phi}_{zz} - \tilde{\phi}_{xz}^2) + \tilde{\phi}_z^2(\tilde{\phi}_{xx}\tilde{\phi}_{yy} - \tilde{\phi}_{xy}^2) \\ + 2[\tilde{\phi}_x\tilde{\phi}_y(\tilde{\phi}_{xz}\tilde{\phi}_{yz} - \tilde{\phi}_{xy}\tilde{\phi}_{zz}) + \tilde{\phi}_y\tilde{\phi}_z(\tilde{\phi}_{xy}\tilde{\phi}_{xz} - \tilde{\phi}_{yz}\tilde{\phi}_{xx}) \\ + \tilde{\phi}_x\tilde{\phi}_z(\tilde{\phi}_{xy}\tilde{\phi}_{yz} - \tilde{\phi}_{xz}\tilde{\phi}_{yy})] \end{Bmatrix}}{(\tilde{\phi}_x^2 + \tilde{\phi}_y^2 + \tilde{\phi}_z^2)^2} \quad (6.2)$$

We can use the scalars obtained and attach them to the vertices of the triangulated surface extracted by the *Marching-Cubes* (see figure 6.13-(b) for the surface extracted). However those values do not give valuable visible information that discriminates the structures we are looking for. We know that those convex structures

have the particularity to have high principle curvatures κ_1 and κ_2 . Knowing that $\kappa_M = \kappa_1 + \kappa_2$ and $\kappa_G = \kappa_1 \times \kappa_2$, we deduce immediately the value of the principle curvatures.

We can map the maximum of κ_1 and κ_2 on the surface of the extracted object, as shown in figure 6.13-(c), but it does not give a clear view of the polyps.

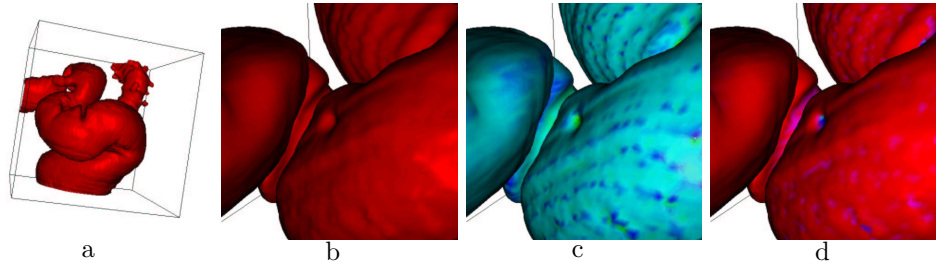


Figure 6.13. Example of polyps visualization: First image: the segmentation obtained by combining Fast-Marching and Level-Sets; second image: a zoom on a region of the colon volume; third image: the mapping of the function of the principle curvatures computed; fourth image: the threshold of this texture which highlights the polyps.

Furthermore, having in mind that we are looking for regions with negative curvatures, we apply the following equation

$$f(\kappa_1, \kappa_2) = \min(\max(\kappa_1, \kappa_2), 0) \quad (6.3)$$

which is interpolated at the vertices of the triangulated surface as shown in figure 6.13-(d). Only the regions where the two principle curvatures are negatives (*cups*) have negative f values, others get null values.

6.2.3 Perspectives

Unfortunately, other non-pathological regions are enhanced. The last row in figure 6.14 displays the result of this curvature mapping for four different datasets. Segmentation step was achieved using the same parameters for each datasets, and the curvature mapping is done with the same color-map. On several datasets, this mapping highlights other non-pathological regions: folds can be highlighted because of the sign of their principle curvatures. However our approach might be consider as a valuable start for the automatic detection of polyps, and currently viewed as an assisting tool for their visualization. The polyps are emphasized, and discriminated from the whole surface. Therefore, segmentation and visualization is achieved with a simple and fast process, leading to a pre-detection of the polyps which can already be used by any clinician.

In conclusion, the use of this kind of curvature filter outputs information relative to small and spherical polyps. Those polyps can grow and develop malignant tumor with non-smooth shapes where the curvature information is not suitable. Our tool finds its application in the early detection of the small polyps. The high precision of

the implicit level-set representation of the surface obtained through the segmentation process, enables to map on the surface informations for small objects like polyps. Our curvature measure is dedicated to this visualization.

Having in mind the settle of a non-supervised method of polyps detection, next step is recognition: Other non-pathological objects that are pre-detected can be discriminated with classification of the shapes of the connected components of the subset of the surface which corresponds to negative values of our function in equation (6.3). In last row of figure 6.14, we can imagine that we are able to unfold the surface of our colon, keeping the curvature information mapped on the explicit representation extracted at convergence of ϕ . This technique has been developed for level-sets techniques by *Hermosillo et al.* [76] using an explicit representation of the surface, with the curvature information mapped onto, which matches the implicit representation during its deformation (in this case, the mean curvature flow to unfold the brain surface, with a constraint on volume conservation). It was also developed in a different manner by *Bertalmio et al.* [12], where the region of interest is tracked as the intersection of two level-sets. Their application is to unfold the cortex in order to see the cerebral activity (mapped onto the surface with a given colormap) in the hidden sulci. Another possible technique is surface warping: using a warping based on registration methods, we can flatten the colon underlying triangulated surface of the zero level-set, into the plane, using a conformal mapping method, as in [73], or another mapping which preserve areas (as done in [74]).

Another possible development is the correct choice for the image scale. The image scale is an important parameter for the aspect of the surfaces and the regularity of the curvatures, but of course large smoothing factors can change the topology of the resulting segmented surfaces. The use of curvature flows seem unadapted as well [44]. A flow based on the intrinsic Laplacian of the mean curvature (see *Chopp and Sethian* [28]) might be an interesting tool to experiment in the future, but the numerical issues related to this flow are still to be explored, and no numerical scheme is currently available.

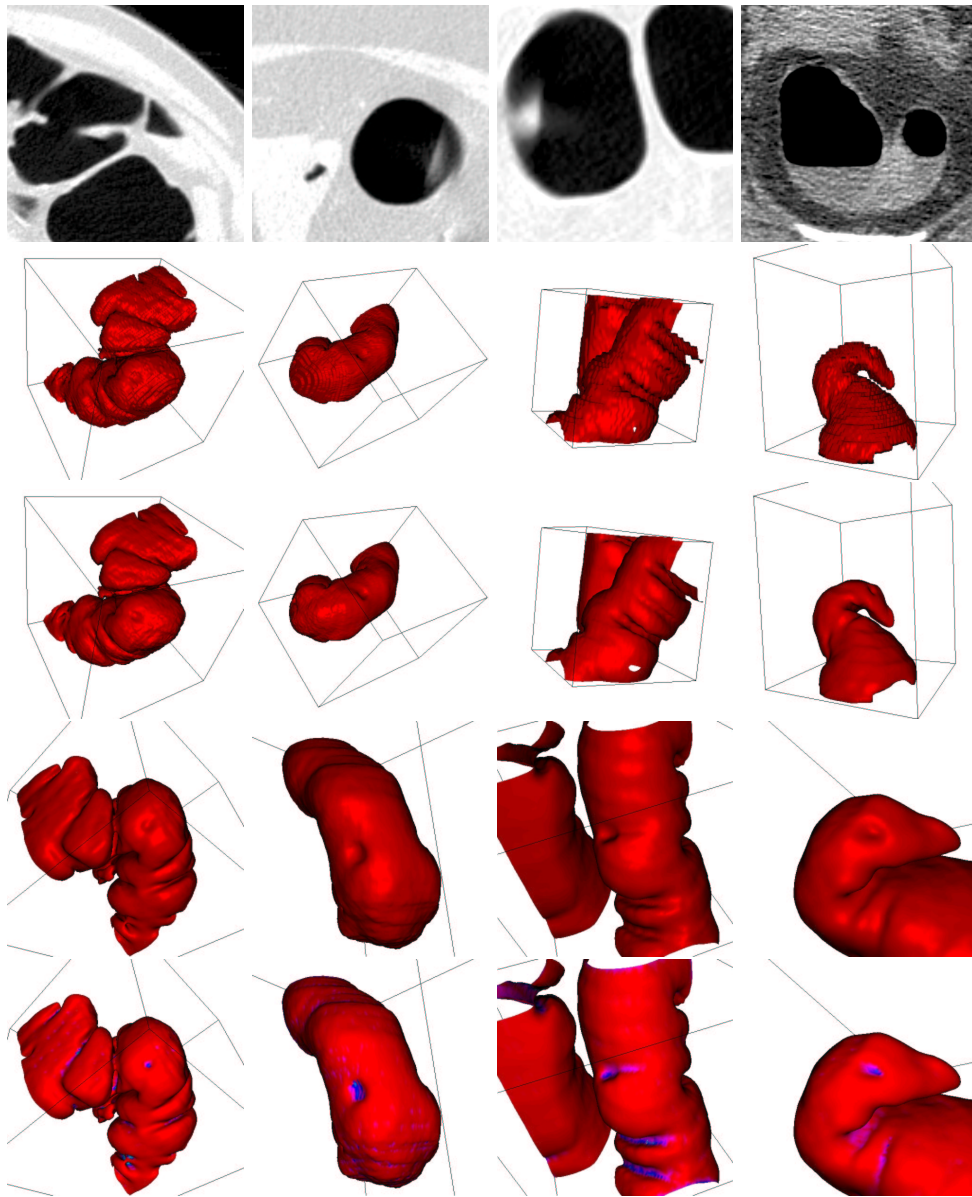


Figure 6.14. Polyps Visualization: First row: the four datasets used for segmentation and visualization; second row: the respective initializations given by the Fast-Marching competition algorithm described in section 5.3; third row: visualization after 20 iterations with region-based forces of the respective zero level-set; fourth row: another point of view for visualizing the polyps; fifth row: texture mapping with the curvature information.